Laser-heating ^{40}Ar/^{39}Ar dating system of the Geological Survey of Japan: System Outline and Preliminary Results

Kozo UTO*, Osamu ISHIZUKA*, Akikazu MATSUMOTO*
Hikari KAMIOKA* and Shigeko TOGASHI*

Abstract: ^{40}Ar/^{39}Ar dating system has been established at the Geological Survey of Japan (GSJ). Main emphasis of the system is to date individual grains of minerals and a few milligrams or less of volcanic rocks using a laser-heating technique. The system consists of four parts; argon isotope laboratory, laser extraction system, noble gas mass spectrometer, and operation desk. The great advantage of the laser extraction system of GSJ is to use the optical glass-fiber and the microscope for the beam path from the laser tube to the sample chamber. This combination makes it possible to create various sizes of laser beam up to 4 mm with homogeneous energy distribution focused on the sample surface. It is, thus, possible to homogeneously heat the sample of a few millimeters in diameter. Preliminary experiments on biotite standards suggest that not only total fusion dating but also stepwise heating experiment of a single to a few grains were successful and gave reliable ages. Relative age relationships between Sori and FC3 biotite standards are perfectly matched with their existing K-Ar ages. Total fusion dating of one or two grains of two biotites from Neogene volcanic rocks gave consistent ages with the existing K-Ar ages. A weighted mean age for 13 analyses on Muro volcanic rocks (K-Ar age: 14.44±0.16 Ma) is 14.31±0.04 Ma, and that for 7 analyses on Utaosa Rhyolite (2.48±0.02 Ma) is 2.52±0.02 Ma. A stepwise heating experiment on a millimeter size groundmass grain of a Miocene volcanic rock (K-Ar age: 9.7±1.6 Ma) was also successful and a very reliable plateau age of 12.09± 0.19 Ma was obtained as a weighted mean of 12 consecutive steps.

1. Introduction

Even though ^{40}Ar/^{39}Ar dating method is a modification of K-Ar method, it has great advantages over the latter. While K-Ar method needs two homogeneously split aliquots of a sample for the quantitative analyses both of potassium and argon to obtain an age, ^{40}Ar/^{39}Ar method gives an age from a single argon isotopic analysis of a sample. This difference has brought ^{40}Ar/^{39}Ar method a wider geochronological application than K-Ar method. For example, ^{40}Ar/^{39}Ar method can provide 1) a precise age information of a single grain mineral and/or a millimeter size rock fragment, 2) a meaningful age for an altered or thermally disturbed rock by the stepwise heating experiment, and 3) information of the possible existence of extraneous ^{40}Ar.

At the Geological Survey of Japan, a three-year term project "Development of the ^{40}Ar/^{39}Ar dating method using a trace amount of sample" was initiated in the fiscal year 1994, and the research has been conducted to establish an ^{40}Ar/^{39}Ar laboratory using the laser-fusion technique. In this paper, we describe the dating system in detail and also report the preliminary results of some age-known samples.

2. Principle of ^{40}Ar/^{39}Ar method

^{40}Ar/^{39}Ar method is a variation of the K-Ar dating method which uses the electron capture decay of ^{40}K to ^{40}Ar (decay constant $\lambda_e = 0.581 \times 10^{-10}$/y). Before the argon analyses, samples are sent to the reactor for the fast-neutron irradiation. A part of ^{39}K in samples are converted to ^{39}Ar by the ^{39}K(n,p)^{39}Ar reaction. As the

*Geochemistry Department, GSJ

^{40}K/^{39}K ratio in natural rocks is constant ($=$ 0.118×10^{-4}), we can estimate the content of ^{40}K in samples through the analysis of ^{39}Ar derived from ^{39}K (^{39}Ar$_K$) if we exactly know how many percent of ^{39}K in samples are converted to ^{39}Ar by the fast neutron irradiation. The age is calculated using the following formula:

$$t = 1/\lambda \times \ln(1 + J \times {}^{40}Ar^*/{}^{39}Ar_K)$$

where $J = {}^{39}K/{}^{40}K \times \lambda/\lambda_e \Delta \int \Phi(E)\,\sigma(E)\,dE$

λ : total decay constant of ^{40}Ar (5.534×10^{-10}/y)

^{40}Ar* : radiogenic ^{40}Ar

^{39}Ar$_K$: ^{39}Ar derived from ^{39}K by the reaction with the fast neutron

Δ : duration of the irradiation

$\Phi(E)$: neutron flux at energy E

$\sigma(E)$: neutron capture cross section at energy E

As it is difficult to precisely know the $\Phi(E)$ and $\sigma(E)$, it is a common practice to calculate the J value from the ^{40}Ar/^{39}Ar analyses of a age-known mineral using the following scheme:

$$J = \{\exp(\lambda t) - 1\}/({}^{40}Ar^*/{}^{39}Ar_K)$$

^{40}Ar/^{39}Ar dating, therefore, is a method to date rocks and minerals relative to the age of a standard mineral.

There are some undesirable interfering argon isotopes produced from Ca K, and Cl by the reaction with neutron. Corrections are made by analyzing synthetic KFeSiO$_4$ glass and fused CaF$_2$ (99.9%CaF$_2$) irradiated together with samples. KFeSiO$_4$ glass was synthesized fusing the mixture of chemicals of K$_2$CO$_3$, Fe$_2$O$_3$ and SiO$_2$ under vacuum at around 900°C. Isotopic ratios of potassium-derived ^{40}Ar to ^{39}Ar and ^{38}Ar to ^{39}Ar were measured by analysis of KFeSiO$_4$. Ratios of Ca-derived isotopes, (^{39}Ar/^{37}Ar) and (^{36}Ar/^{37}Ar), were determined by analysis of CaF$_2$. These ratios are measured for each irradiation. Interfering ^{36}Ar and ^{38}Ar derived from ^{35}Cl and ^{37}Cl are small enough to ignore for the normal rocks and minerals.

3. Outline of the Laser ^{40}Ar/^{39}Ar dating system

The experimental system for laser ^{40}Ar/^{39}Ar dating can be divided into the following four parts: 1) laboratory room to handle radioactive materials, 2) laser extraction system, 3) high-sensitivity noble gas mass spectrometer, and 4) operation desk. In the following, details of each facility are described.
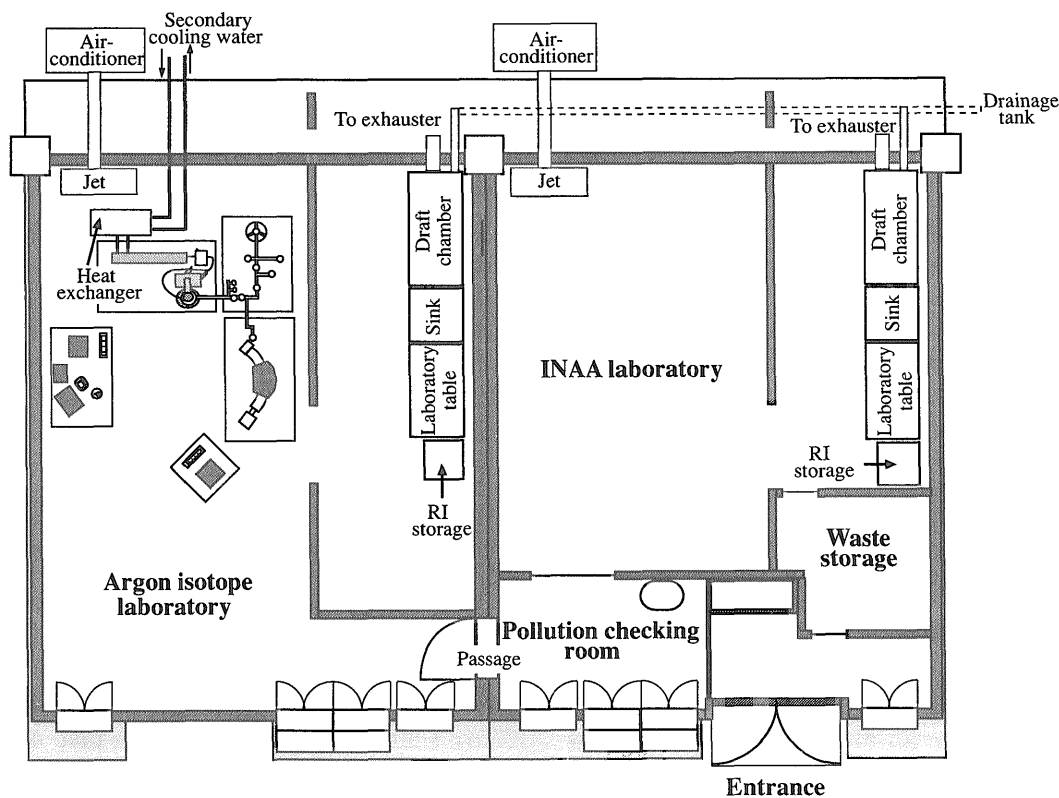

Fig. 1 Outline of Argon isotope laboratory.
Argon isotope laboratory and instrumental neutron activation analysis (INAA) laboratory compose a single restricted area regulated by the law, but they work as independent laboratories.
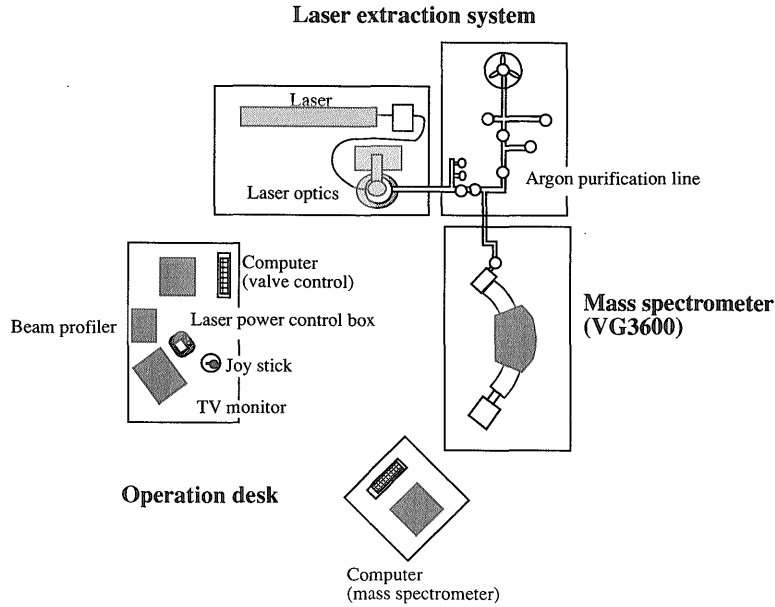
Laser extraction system

Laser

Laser optics

Argon purification line

Computer
(valve control)

Beam profiler

Laser power control box

Joy stick

TV monitor

**Mass spectrometer
(VG3600)**

Operation desk

Computer
(mass spectrometer)

Fig. 2 Configulation of $^{40}Ar/^{39}Ar$ experimental instruments.

CCD camera

Dichroic mirror

Beam profiler TV monitor

Optical fiber

Ar-ion laser

Fiber
coupler

Objective
lens

Sample chamber
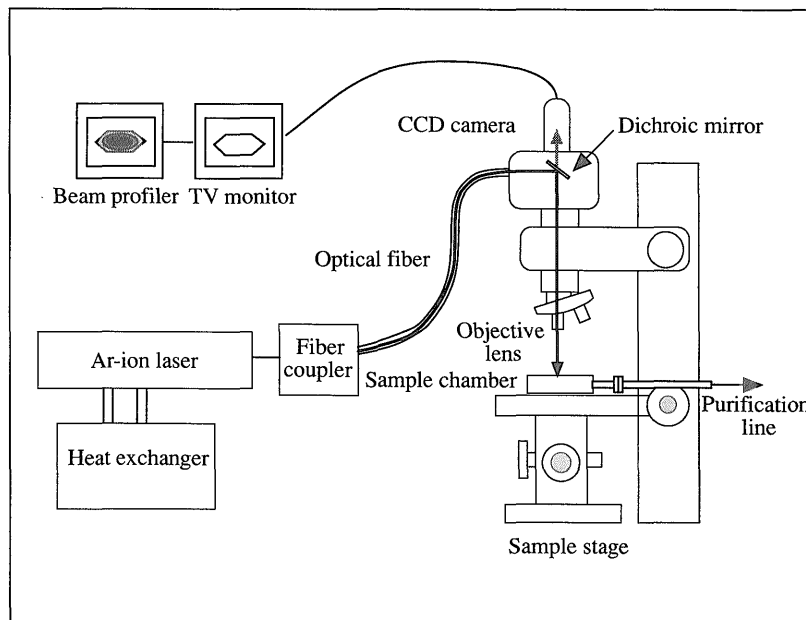
Purification
line

Heat exchanger

Sample stage

Fig. 3 Configuration of the argon-ion laser and laser optics.

Laser beam emitted from a 10W continuous Ar-ion laser is introduced to the optical fiber cable connected to the optical microscope. Then, the beam comes out of the objective lens and passes through the viewport of the ultra-high vacuum sample chamber to heat the sample inside.

3.1 Argon isotope laboratory

The rock and mineral samples to be dated by $^{40}Ar/^{39}Ar$ method are sent to a reactor for the irradiation of fast neutron before the dating experiment. In the reactor, analyzed samples are exposed to the fast neutron for about 24 hours in order to change ^{39}K into ^{39}Ar by the ^{39}K (n,p)^{39}Ar reaction. Samples sent back from the reactor after the irradiation are necessary to be

treated inside a special laboratory that is regulated by the law. The outline of the argon isotope laboratory is shown in Fig. 1. The room is constructed as an annex to the existing Instrumental Neutron Activation Analysis Laboratory, and two rooms are treated as a single restricted area; that is, having a common entrance, a pollution checking facility, radioactive-waste depository and a water drain cham-

ber. They, on the other hand, have independent air circulation systems, depositories of radio-active materials, draft chambers and sinks, and thus work as independent laboratories.

3.2 Laser extraction system

Laser extraction system consists of an argon-ion continuous laser, laser optics, sample chamber and argon purification line (Figs. 2 and 3).

The laser is a 10W continuous argon-ion laser, Coherent INNOVA300 model. Used wave-lengths are 488 and 514 nm in a visible wave area, and blue-colored beam is emitted.

A laser optics consists of laser coupler, optical glass-fiber and optical microscope. Laser beam emitted from the laser tube is immediately cou-pled into an optical fiber through a laser cou-pler, and then fed into a microscope. Inside the microscope, the laser beam is reflected by mir-rors and it comes out through an objective lens. The beam finally falls perpendicularly into the sample chamber. The microscope has no eye lens for the safety reason, instead equips CCD camera on top, and the sample image can be safely monitored on the TV monitor screen set on the operation desk. The mirror just between the objective lens and the CCD camera reflects the light of visible wavelengths nearly 100%, but let infrared light pass through it. Therefore, only the light of near-infrared or longer wave-lengths from the sample can be sampled by the CCD camera, and the monochrome image is observed by the TV monitor. The sample stage of the microscope has three step-motors which enable X, Y and Z movements independently by the remote control operation.

The sample chamber is made up with a $\phi70$ mm UHV view-port, housing, sample holder and a glass cover, and is connected to the argon purification line by a $\phi32$mm ICF flange (Fig. 4). The sample holder is a copper disk of 35 mm in diameter and 5 mm in thickness, and 16 or 54

holes, 2-3 mm across and ~2mm deep, are drilled on it. A single to a few grains of rock and mineral samples are placed in each hole. The cover glass put on the holder is a 2mm thick Pyrex glass, and is used to prevent the spillover of sample from the hole and the scattering of melts during the sample fusion. A laser beam emitted from the objective lens penetrates into the ultra-high vacuum chamber through the viewport, and hits and heats samples. Heated samples then release gases including argon, and the gases diffuse into the purification line.

The outline of the argon purification line is shown in Fig. 5. Main line is made of stainless steel tubes of 8 μm inner diameter. A part of the line is a flexible tube which enables the smooth movement of the sample holder on the motor-controlled XYZ-stage. In order to purify and extract argon from the released gases from the sample, two getter pumps are attached in paral-lel to the line. They are Zr-Al alloy getters encapsulated into Pyrex glass tubes (SAES AP-10) whose nominal pumping speed is 10l/s. One of them is kept at about 450°C to adsorb mainly hydrocarbons, nitrogen, carbon-monoxide and carbon-dioxide, and the other is to adsorb mainly hydrogen at room temperature. There are two pumping lines to achieve very clean ultra-high vacuum, one is a 60 l/s turbo-molecu-lar pump with a 33 l/s oil-rotary roughing pump and the other is a 30 l/s ion pump. The former pumps are used for rapidly pumping from the atmospheric pressure to 10^{-9} mbar during the bakeout at 200-300°C, while the latter is for the final achievement of ultra-high vacuum of the order of 10^{-10} mbar. There are a few valves, capable of the high-temperature bakeout up to 350°C, to isolate pumps and partition the line. Two of them, one is between the ion pump and the line and the other between the mass spectrometer and the line, are attached with
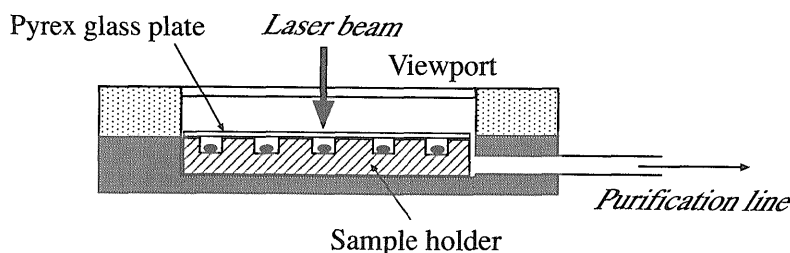

Fig. 4 Schematic cross section of sample chamber.

Copper-made sample holder is placed in the sample chamber and covered with Pyrex-glass plate. Samples are loaded in holes drilled on the copper disk. The sample chamber is evacuated to ultra-high vacuum. Laser beam penetrates into the ultra-high vacuum sample chamber through the glass viewport of the sample chamber and heats samples.
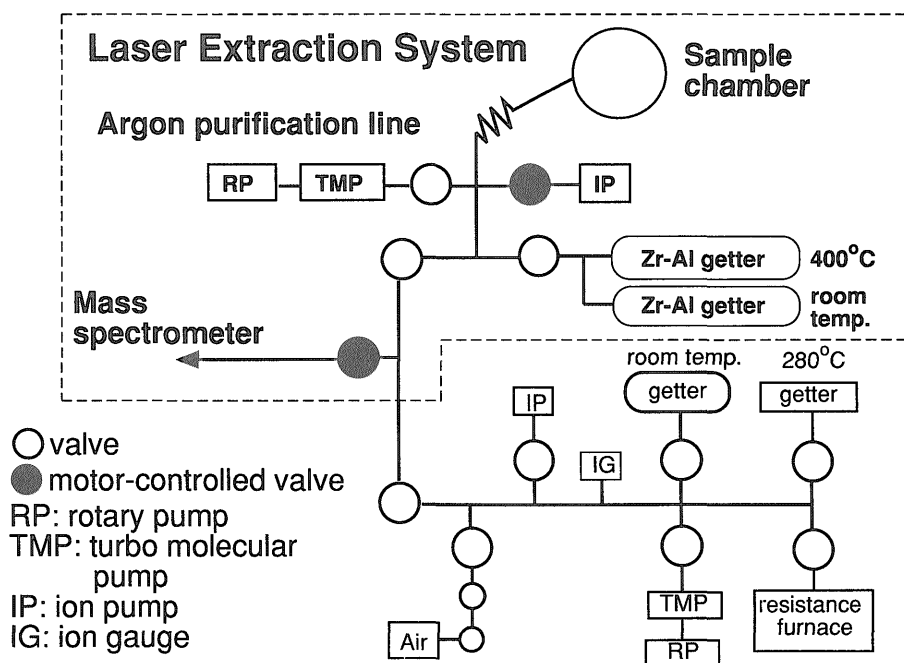
Fig. 5 Schematic diagram of the argon purification line.
  Gases released from the sample are introduced into the argon purification line and are exposed to two Zr-Al getters. The area surrounded by dashed line is used for laser-fusion analysis. The area outside the dashed line is designed for the experiments using a resistance furnace in the future.

torque motors which enable the remote operations of these valves.

In addition to the laser argon purification line, there is an annex line of the resistance furnace for the precisely temperature-controlled heating experiments for larger amounts of samples. This line is equipped with independent cleanup and pumping systems to prevent the cross-contamination of active gases between the two extraction lines. The resistance furnace is under development and will be used in the future.

The sample chamber and two extraction lines can be baked all together up to 350°C inside the oven. The oven is raised above the line by the wire winch during the normal operation of lines.

3.3 Noble gas mass spectrometer

Argon gas extracted and purified from the sample in the laser extraction line is directly introduced into the mass spectrometer through the inlet valve. The mass spectrometer, VG Isotech VG3600, is specially designed for noble gas analyses, equipped with two collectors; a Faraday collector for the larger amounts of ions, and a Daly collector for the smaller amounts of ions. Combination of two collectors enables the wide dynamic range of argon measurements. The Daly collector, mostly used for the laser $^{40}Ar/^{39}Ar$ analyses, consists of Daly knob (conversion electrode), scintillator and

photomultiplier. Ions transmitted through the exit slit of the flight tube are deflected 90 dgrees by the negative potential (-10 kV) and impacted to the surface of the Daly knob. The secondary electrons ejected from the knob are scattered on to the scintillator, in which electrons are converted into photons, and then photons are amplified by the photomultiplier (Potts, 1987). The big advantage of this collector over the secondary electron-multiplier, normally used to detect small amounts ion beams, is the perfect linearity between the amount of incoming ion beams and the output voltage. Consequently, there is no change in measured isotopic ratios regardless of the sample size. Currently, the sensitivity of the Daly collector is adjusted about 100 times against the Faraday collector, and its detection limit for ^{40}Ar is about 10^{-15} mlSTP (10^{-18} mole). The blank of the system including mass spectrometer and the extraction line is currently 4.5×10^{-14} mlSTP for ^{36}Ar, 2.8×10^{-13} mlSTP for ^{37}Ar, 2.0×10^{-14} mlSTP for ^{38}Ar, 4.0×10^{-14} mlSTP for ^{39}Ar, and 1.5×10^{-12} mlSTP for ^{40}Ar. As a single plagioclase grain of 1 Ma (assuming $\sim$1mg, $K_2O = 0.3$wt.% and non-radiogenic $^{40}Ar = 5 \times 10^{-8}$ mlSTP/g) contains 1.6×10^{-13} mlSTP of ^{36}Ar and 6×10^{-11} mlSTP of ^{40}Ar, the current $^{40}Ar/^{39}Ar$ system has the potential to measure a single plagioclase grain younger than
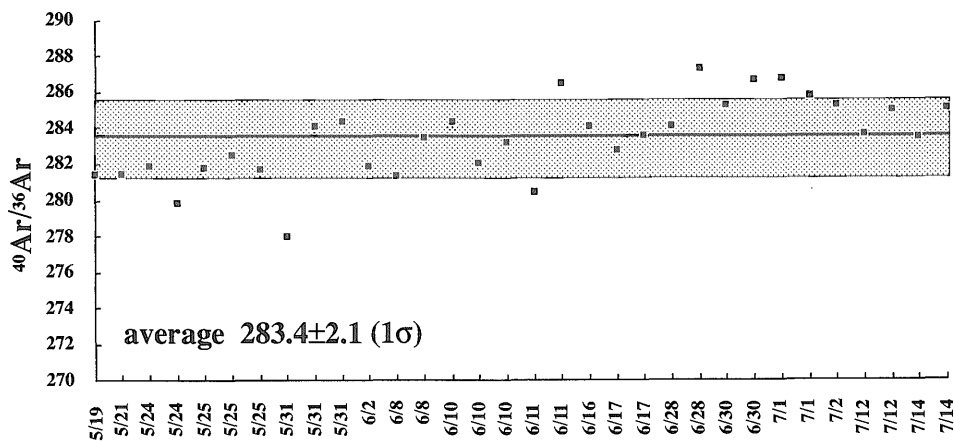
Fig. 6 Temporal variation of atmospheric $^{40}Ar/^{36}Ar$ ratio analyzed using the Daly collector during 2 months.

1 Ma.

The average of atmospheric $^{40}Ar/^{36}Ar$ ratios (twenty-one analyses during one month) analyzed using Daly multiplier is 283.4±2.1 (Fig. 6). This indicates a reproducibility of 0.74% (1 σ) for the $^{40}Ar/^{36}Ar$ ratio. Obtained ratios are somewhat discriminated from the known atmospheric ratio (295.5; Nier, 1950). In the actual sample analyses, measured isotopic ratios are corrected for mass discrimination in a way described in Appendix 1.

3.4 Operation desk

This analytical system potentially has two kinds of risk to the human health, one is handling radioactive materials and the other is using laser. Samples loaded in the sample chamber are about a few tens of milligrams in total, thus radiation dose from samples is negligible. The laser beam almost runs inside the optical system and is barely exposed outside the optics, only between the objective lens and the sample chamber. In addition, the whole laser optics sit inside a safety box. There is , therefore, almost no possibility of the human hazard. We, however, added an additional safety, that is, the operation desk on which all the necessary experimental work can be done by the remote control (Fig. 2). The operational desk is located away from the laser extraction system, and the operator is able to proceed experiments turning his or her back to the system.

On or in the operation desk, all necessary control devices are gathered. They are 1) optics control box, 2) XYZ-stage control box and the joystick, 3) laser power control box, 4) TV monitor, 5) torque motor control box for the manual valve operation, 6) computer for the automatic operation mainly of sequential valve operations, and 7) beam profiler for the thermal

energy monitoring.

3.5 Advantage of a laser optics using optical glass-fiber

In our laser $^{40}Ar/^{39}Ar$ dating system, we use optical glass-fiber for the laser beam path which is very unique comparing with other laser $^{40}Ar/^{39}Ar$ dating systems in the world. This enables us to create a large wide beam up to a few millimeters in diameter with homogeneous energy distribution, and thus makes it possible to heat a millimeter size sample homogeneously. This is very essential to perform the stepwise heating experiment of volcanic rocks by the laser heating facility (Fig. 7).

In many laboratories, for example at USGS Menlo Park, the laser beam passes through the
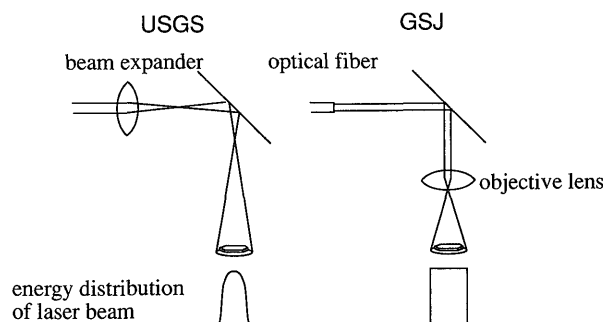

Fig. 7 Comparison of the laser optics between GSJ and USGS.

In order to heat a large size (>1mm) sample, the defocused beam with Gaussian-like energy distribution is emitted to the sample in the experimental system like USGS, Menlo park. The laser optics of GSJ, on the other hand, can create the focused laser beam up to 4mm in diameter with the flat energy distribution.

air, and is reflected by the combination of mirrors (Dalrymple, 1989). The binocular and the CCD camera for the observation of samples are set obliquely not to disturb the beam path. In case of the total fusion of a sample, it is easy to focus a narrow laser beam on the sample surface and increase the laser power until fusing a sample. On the other hand, it is difficult to heat the entire sample homogeneously, which is essential for the stepwise heating experiment. In order to heat a sample larger than a few hundred micrometers in diameter, it is necessary to defocus the laser beam to expand its diameter. In that situation, the energy distribution across the beam becomes Gaussian; i.e., the highest energy in the center of the beam while decreasing toward the margin (Pringle *et al*., 1992). The sample exposed to such a beam is not heated evenly, and the temperature of the sample also decreases toward the margin. This is fatal for the precise stepwise heating of a chronologically heterogeneous sample, and an artificial age spectrum may be formed due to the inhomogeneous heating of a sample (Stewart *et al*., 1996).

In case of the laser optics of the Geological Survey of Japan, the combination of optical glass-fiber and a microscope enables to create an energetically homogeneous laser beam with a variety of diameters (Table 1). The laser beam randomly scatters inside the optical fiber, and an energetically homogeneous beam of the same diameter as the inner diameter of the fiber is created when it comes out of the fiber. The optical microscope creates the focused image of such a laser beam on the surface of sample just when the image of the sample is focused on the CCD camera. Thus, we can create a focused beam with homogeneous energy with various diameter by just changing the diameter of the glass-fiber and the magnification of the objective lens. With increasing the diameter of the glass-fiber and decreasing the magnification of the lens, the diameter of the beam increases (Table 1). Since some scattering of the beam

occurs when the beam penetrates through the viewport glass and the cover glass above samples, we observe a certain drop of the energy of the beam along the peripheral of the beam. Nevertheless, we overcome this by making the beam diameter considerably larger than the sample. We can confirm the homogeneous temperature distribution across a sample by the observation of the image of the beam profiler. Stepwise heating experiments using this laser optics system should be a big advantage in the future.

4. $^{40}Ar/^{39}Ar$ experimental procedures

4.1 Neutron irradiation

Samples used for $^{40}Ar/^{39}Ar$ experiments are grains of minerals and rock fragments, about 0.25-1mm in diameter. Several grains of a sample were wrapped in an aluminum foil packet about 8mm x 8mm in size, and the packets were piled up in a pure aluminum (99.5%Al) capsule (13mm in outer diameter with a wall thickness of 1.5 mm and 40 mm long) along with $KFeSiO_4$ and CaF_2 monitors (Fig. 8). Age known standard minerals were placed with every three or four packets of unknown samples (about 5mm

Table 1 beam size selection

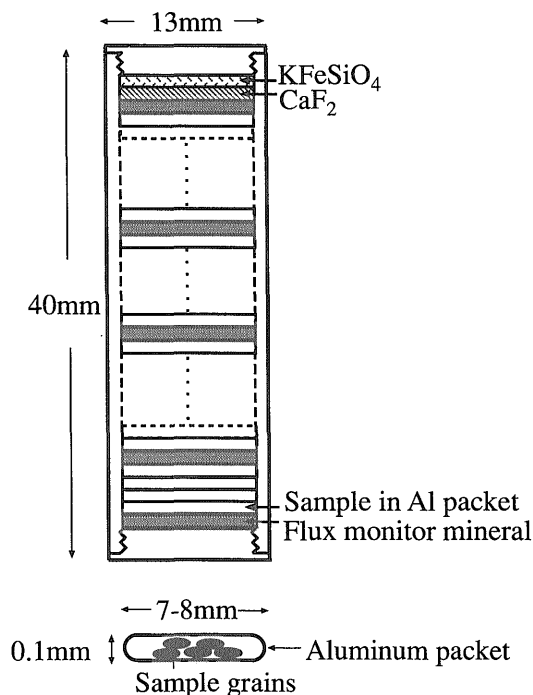| Beam size(μm)		Diameter of optical fiber(μm)			
		400	200	100	50
Magnification of objective lens	x2	4000	2000	1000	500
	x5	1600	800	400	200
	x20			100	50
	x50			40	20

Fig. 8 Schematic cross section of the aluminum capsule for the neutron irradiation.
Samples wrapped in an aluminum foil are piled up in a pure aluminum capsule. Unknown samples are sandwiched between flux monitor minerals.

interval) as the neutron flux monitors. In the current studies, sanidine and biotite separates from the Fish Canyon tuff from Colorado, U.S. A. were used as the flux monitor minerals. The sample (FC3) was collected by Dr. M. Kasuya from the same locality of the sample from which the international zircon and apatite standards for fission-track dating were separated (Naser and Cebula, 1985). The K-Ar age of FC3 biotite was carefully determined by both the isotopic dilution and sensitivity methods at GSJ. The weighted average of six analyses by the isotopic dilution method is 27.5±0.2 Ma and that of 9 analyses by the sensitivity method is 27.4±0.2 Ma (Uto *et al.*, unpublished data). These ages agree well with the $^{40}Ar/^{39}Ar$ sanidine age of 27.55±0.12 Ma determined at USGS Menlo Park (Lanphere *et al.*, 1990). In this study, we fixed the age for FC3 sanidine and biotite to be 27.5 Ma in order to calculate the J values.

The aluminum capsule was further wrapped with 0.8mm-thick Cd-foil in order to minimize undesirable reactions caused by the irradiation of thermal neutron. This Cd shield can capture more than 98% of thermal neutron before penetrating into the capsule. Samples were irradiated for 24 hours at HR1 position of the hydraulic rabbit irradiation facility of the 50MW Japan Materials Testing Reactor (JMTR), Oarai Research Establishment, Japan Atomic Energy Research Institute. Neutron flux in this facility is about $6.7 \times 10^{12} n/cm^2 s$ with maximum of $8.8 \times 10^{12} n/cm^2 s$ for fast neutron and $8.1 \times 10^{13} n/cm^2 s$ with maximum of $1.1 \times 10^{14} n/cm^2 s$ for thermal neutron (JMTR handbook, 1994). Temperature

of samples at irradiation was estimated to be lower than 150°C (Minoru Narui, personal communication).

4.2 Argon isotope analysis

One to a few grains of irradiated minerals or volcanic rocks were placed in a hole on the sample holder and then evacuated to ultra high vacuum. Samples were baked at 200°C for 30-40 hours to remove gas adsorbed on the surface of the purification line and samples. First, the sample image taken by the CCD camera on top of the microscope is monitored on the screen of the TV monitor, and the location of the sample and the focus of its image is adjusted using the XYZ stage controller. Then, the operator starts the valve control program of the computer to sequentially open or close three valves of the extraction line and the mass spectrometer. The shutter of the laser beam is opened and the laser beam is exposed to the sample. The power of the laser is gradually increased by observing the sample image on the screen. The relative temperature distribution of the sample can be monitored by the beam profiler image. After heating samples for two to three minutes and purifying extracted gases with two Zr-Al getters for another seven minutes, the argon gas is introduced to the mass spectrometer by the computer's valve operations. The argon isotopic measurement with the mass spectrometer is operated by another computer located next to the mass spectrometer.

Before analyzing extracted gas from samples, blank analyses were made regularly. In the blank analyses, all the experimental procedures

Table 2   Analytical procedure of mass spectrometry for Ar isotope analysis

No.	Mass	Integration time (second)	Comment
1	35.5	7	Dummy
2	36	6 (6)	^{36}Ar peak
3	37	6 (6)	^{37}Ar peak
4	38	4 (4)	^{38}Ar peak
5	38.5	10 (10)	Background
6	39	6 (6)	^{39}Ar peak
7	40	6 (6)	^{40}Ar peak

Numbers in parentheses are integration time for blank analysis

Dummy analysis at Mass 35.5 is to reduce the effect of "tailing"

after the measurement of the large ^{40}Ar peak.

are the same as the actual sample analyses except for no heating of samples by the laser probe. Total blank including the mass spectrometer and the extraction line, as already mentioned in chapter 3.3, is similar to the blank of the mass spectrometer alone.

In the actual sample analyses, the laser heating procedure is slightly different between total fusion and stepwise heating analyses. In the total fusion analyses, samples were fused completely within a minute or two with a narrow laser beam. In the stepwise heating analyses, samples were heated for 2 or 3 minutes with the designated laser power. The beam size of the laser was kept bigger than the diameter of samples. Experimental procedures are as follows. We isolate the extraction line from the ion pump, and heat or fuse samples as described above, and the line was held in static vacuum for another 7 or 8 minutes in order to adsorb active gases with hot and cold getters . We then close the ion pump of the mass spectrometer, open the inlet valve between the extraction line and the mass spectrometer, and start the analytical program. Eleven sets of sequential measurements of five argon peaks (mass 36, 37, 38, 39 and 40) and a background at mass 38.5 were repeated (Table 2). Net intensity of each Ar peak and net $^{39}Ar/^{40}Ar$ ratio were extrapolated to the zero time when the argon gas was introduced into the mass spectrometer. After correcting the blank, J values and ages were calculated for the standard and unknown samples, respectively, using the formulas described in Appendix 1.

5. Preliminary results

Preliminary $^{40}Ar/^{39}Ar$ analyses have been made on some mineral separates and volcanic rocks whose ages have been well known by K-Ar method. First, we determined J values, which are essential to calculate ages of samples, by repeatedly analyzing the age standard minerals, FC3 sanidine and biotite. Next, we compared the results of single grain total fusion analyses of two standard biotites, and confirmed the reliability of our experimental procedure. We, then, performed total fusion analyses of two age-known biotite samples and confirmed the consistency between total fusion $^{40}Ar/^{39}Ar$ and K-Ar ages. We, further, proceeded to the stepwise heating experiments on the Sori biotite and the Miocene volcanic rock, and examined the age spectra of these samples.

5.1 Determination of the J value

As was mentioned in chapter 2, age-known standard minerals are used to know the J value in order to calculate ages of unknown samples. As neutron flux changes considerably across the capsule, we should sandwich the unknown samples with the standards to interpolate the J value at the position of each unknown sample. In this study, we used FC3 sanidine and biotite as primary neutron flux monitor minerals by assuming their ages to be 27.5 Ma.

The FC3 sanidine and biotite were placed in 7 positions along with unknown samples. Measured J values are shown in Fig. 9 along the vertical direction in the capsule. Except for the FC3 biotite at 4 mm, analytical results form Gaussian like distributions and the weighted mean values are at the middle of the distribution. The FC3 biotite at 4 mm is an exception having two split distributions and the weighted average is in the middle of the two distributions. One possible explanation is the horizontal variation in J value due to the lateral gradient in the fast neutron flux which we recently found.

The weighted mean value of 5 to 10 measurements at each position changes as much as 4.4% from 3.761×10^{-3} to 3.595×10^{-3} over a distance of 23 mm. Relative analytical error of the weighted mean for each standard ranges from less than 0.1% to 0.3%. Two pairs of FC3 biotite and sanidine locate very close each other; those at positions 2 and 5 and those at positions 20 and 21 (Fig. 9). These pairs have consistent J values and agree with each other within ±0.15%. This support the reliability of our analyses and our estimation of the analytical uncertainties.

The variation of J value along the capsule is obviously not a linear change, but there is a sharp change between 11mm and 13.5mm. There is no systematic change between the lower 4 positions, and there is a slight decrease with increasing the height in the upper 3 position. In this study, we calculated the J value at each unknown position by interpolating the values of the nearest upper and lower standards instead of calculating mathematically using nonlinear least square fitting procedure using all standards. As mentioned above, we recently found a considerable variation of J values along the horizontal direction. Since we did not consider the horizontal offset of the locations of samples, it might be the reason for the irregular variations observed in Fig. 9. Further investigations are in progress.

Since all the unknown samples analyzed in this study locate very close to the monitor standards (Fig. 9), the calculated J values should not be much different from those of the standards nearby. We, therefore, estimated the uncertainties of J value for each sample to be 0.2%.
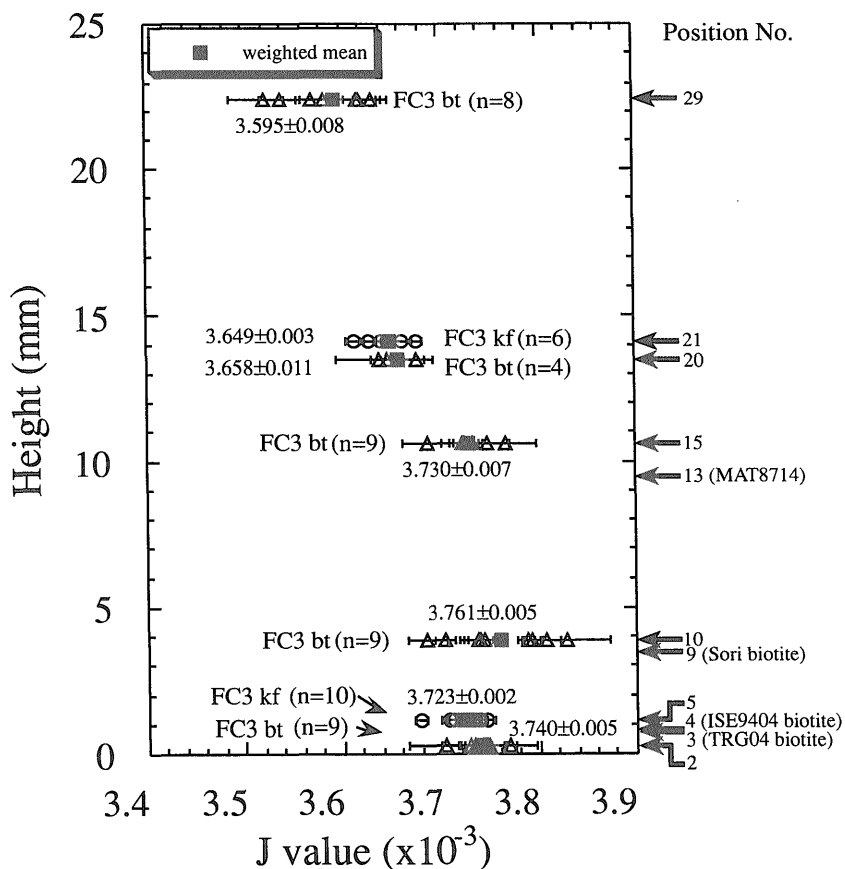
Fig. 9 Variation of J value along the irradiation capsule.
        Error (1s) for each analysis is indicated by a solid bar. FC3 bt and FC3 kf stand for biotite and K-feldspar separated from the Fish Canyon tuff, respectively. J values determined for each monitor position are shown. Positions of each sample in an aluminum capsule are indicated outside the plot.

Table 3 Analytical data for total fusion analysis of FC3 biotite (position No. 2)

$^{40}Ar/^{39}Ar$	$^{37}Ar/^{39}Ar$ (x10⁻³)	$^{36}Ar/^{39}Ar$ (x10⁻³)	$^{37}Ar_{Ca}/^{39}Ar_K$ (x10⁻³)	$^{40}Ar*$ (%)	$^{40}Ar*/^{39}Ar_K$	J value (x10⁻³)
4.890±0.029	19.55±0.31	2.667±0.069	19.55	83.9	4.101±0.033	3.746±0.030
4.439±0.006	76.56±0.60	1.174±0.053	76.57	92.4	4.098±0.017	3.749±0.015
4.558±0.027	28.57±0.39	1.633±0.056	28.57	89.5	4.075±0.031	3.769±0.028
4.580±0.002	20.15±0.34	1.603±0.033	20.15	89.7	4.106±0.010	3.741±0.009
5.144±0.006	16.43±1.68	3.518±0.076	16.43	79.8	4.103±0.023	3.744±0.021
4.714±0.006	11.79±0.61	2.007±0.044	11.79	87.4	4.119±0.014	3.729±0.013
4.889±0.005	25.18±1.33	2.624±0.059	25.18	84.2	4.113±0.018	3.734±0.016
4.438±0.004	55.07±0.92	1.159±0.058	55.07	92.4	4.099±0.018	3.747±0.016
4.802±0.004	9.937±2.332	2.208±0.140	9.937	86.4	4.147±0.042	3.703±0.037

Weighted mean **3.740±0.005**

27.5 Ma was used as the age of FC3 biotite for the caluculation of J value.

Corrected for decay and blank. All errors listed at the 1σ level.

$(^{40}Ar/^{39}Ar)_K$=0.003258±0.001700; $(^{38}Ar/^{39}Ar)_K$=0.05692±0.00027

$(^{39}Ar/^{37}Ar)_{Ca}$=0.0008370±0.0000069; $(^{36}Ar/^{37}Ar)_{Ca}$=0.0003669±0.0000020

5.2 Single grain total fusion analyses of standard minerals

Single grain total fusion $^{40}Ar/^{39}Ar$ analyses were repeated on two standard minerals in order to evaluate 1) the reproducibility of age analyses of our system and 2) the homogeneity of our standard minerals. One is FC3 biotite, our current primary standard, and the other is Sori biotite, an in-house standard mineral of the GSJ K-Ar laboratory (Uchiumi and Shibata, 1980). Each analyzed mineral was 20-30 μg in weight and 200-300μm in diameter.

Table 3 shows the results of 9 analyses of FC3 biotite. Since this mineral was a flux monitor standard with its fixed age of 27.5 Ma, J values calculated from each grain were compared. Calculated J values range from 3.703-3.769× 10^{-3} and none is discordant exceeding the 1σ analytical uncertainty. If we exclude the highest and lowest values which have large analytical uncertainties, J values concentrate in a narrow range of 3.729 to 3.749×10^{-3}, about 0.6% deviation. Since typical relative uncertainty for each grain is 0.4 to 1%, this deviation is very reasonable and suggesting analytical reliability. The weighted average of all 9 analyses is (3.740± 0.005)x10^{-3}. The solid line in Fig. 10a is the probability density distribution spectrum obtained by the sum of the Gaussian probability distribution of each analysis based on its analytical uncertainties. An important advantage of this spectrum is that it incorporates the error of each analysis. The spectrum of J values is almost symmetrical (Fig. 10a) and shows a Gaussian-like distribution. This clearly indicates that all of the analyzed grains are homogenous in age and that all analytical results are acceptable within their estimated uncertainties. The calculated weighted average and its error are considered to be statistically meaningful. We, thus, can conclude that our laser $^{40}Ar/^{39}Ar$ system is capable of analyzing single grain minerals with the uncertainty less than 0.5 %.

Table 4 displays results of 10 analyses of Sori biotite. A packet of Sori biotite was placed just below that of FC3 biotite, being in contact with each other. Therefore, the average J value calculated for FC3 biotite was applied to calculate the age of each Sori biotite grain. As the radiogenic ^{40}Ar signals from a single grain of Sori biotite was too large for the analyses by the Daly collector, extraction and analyses for most grains of the biotite were divided into two temperature steps. The most results shown in Table 4 are the integration of the two fractions. Weighted average age for all analyses is 92.04± 0.18 Ma, which is identical to the K-Ar age of this biotite (91.2±0.6 Ma: Uchiumi and Shibata, 1980) within 2σ analytical error. That indicates that relative age relationships between FC3 and Sori biotites determined by the $^{40}Ar/^{39}Ar$ method is consistent with that by the K-Ar method.

Ages of all individual grains agree well with the weighted mean value considering 2σ uncer-

Table 4   Analytical data for total fusion analysis of Sori biotite (posion No. 9)

$^{40}Ar/^{39}Ar$	$^{37}Ar/^{39}Ar$ (x10^{-3})	$^{36}Ar/^{39}Ar$ (x10^{-3})	$^{37}Ar_{Ca}/^{39}Ar_K$ (x10^{-3})	$^{40}Ar^*$ (%)	$^{40}Ar^*/^{39}Ar_K$	Age (Ma)
14.35±0.01	1.718±0.927	1.474±0.144	1.718	97.0	13.91±0.04	91.86±0.34
14.22±0.01	887.5±1.4	0.8926±0.0592	888.0	98.4	13.99±0.02	92.34±0.22
14.08±0.01	19.33±0.24	0.6443±0.0454	19.33	98.7	13.89±0.02	91.70±0.20
14.53±0.02	8.329±1.041	1.810±0.190	1.810	96.3	13.99±0.06	92.31±0.41
14.37±0.02	10.55±2.67	1.082±0.118	10.54	97.8	14.04±0.04	92.66±0.31
14.49±0.02	3.182±3.727	1.537±0.143	3.182	96.9	14.03±0.05	92.63±0.36
14.09±0.01	19.88±2.65	0.8747±0.0984	19.88	98.2	13.82±0.03	91.27±0.26
14.29±0.02	9.530±3.321	1.120±0.132	9.532	97.7	13.96±0.04	92.15±0.33
14.21±0.02	2.738±1.722	0.7892±0.0653	2.738	98.4	13.98±0.03	92.25±0.25
14.16±0.05	15.91±1.83	0.7993±0.0506	15.91	98.3	13.92±0.04	91.90±0.30
					Weighted mean	**92.04±0.18**

J=0.003754±0.000008

Corrected for decay and blank. All errors listed at the 1σ level.

$(^{40}Ar/^{39}Ar)_K$=0.003258±0.001700; $(^{38}Ar/^{39}Ar)_K$=0.05692±0.00027

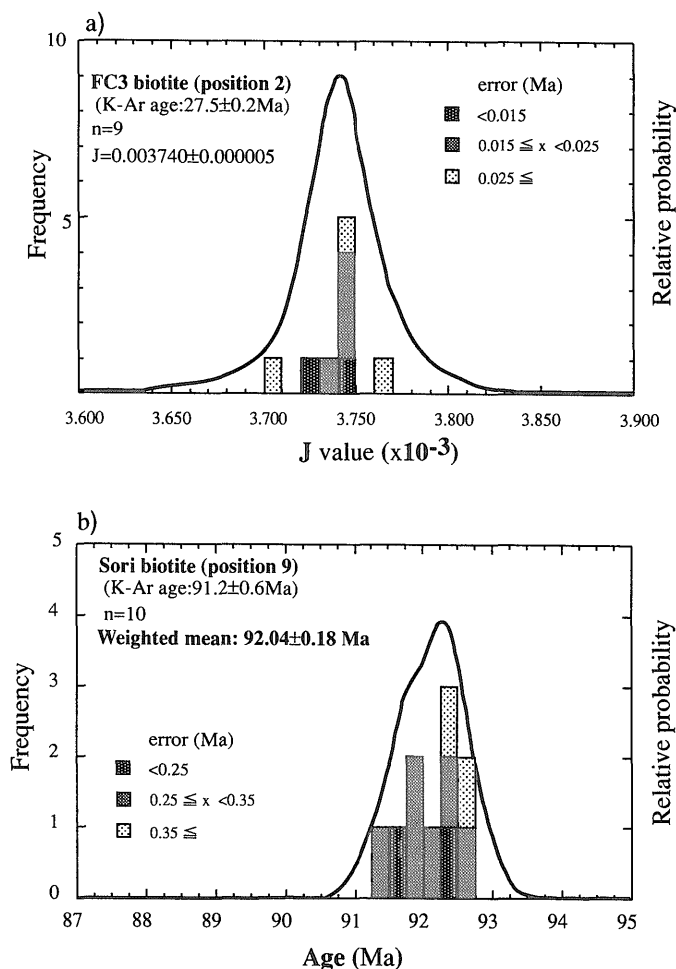$(^{39}Ar/^{37}Ar)_{Ca}$=0.0008370±0.0000069; $(^{36}Ar/^{37}Ar)_{Ca}$=0.0003669±0.0000020

Fig. 10   Results of total fusion analyses of single grain biotite. a) FC3 biotite, b) Sori biotite
a) shows the frequency distribution of J value determined from the analyses of FC3 biotite whose age is 27.5 Ma. b) indicates the age distribution spectrum of Sori biotite. Solid curves depict relative probability distribution spectrum.

tainties. Looking in detail the analytical results (Table 4, Fig. 10b), however, ages for individual grains of Sori biotite scatter much larger range from 91.3 to 92.66 Ma than expected from the analytical error for each grain. The relative probability spectrum, thus, forms a more wider distribution than that for FC3 biotite (Fig. 10). There exists a bump on the younger age side. Two explanations for this broad distribution may be possible. One is a heterogeneity in age of individual biotite grains. Microscopic observation revealed that Sori biotite is partly chloritized along its cleavages and the degree of chloritization is somewhat different grain by grain. If chloritized parts have different ages from the fresh parts, ages may vary between grains according to the degree of chloritization. As will be mentioned in the following section of stepwise heating results, Sori biotite gave younger ages

in the lower temperature steps probably due to chloritization of the biotite. The grains with higher proportion of chloritized part would be younger than the grains poorer in chlorite. Another possibility is a horizontal heterogeneity of neutron flux during the irradiation in the reactor. Since a single packet had the dimension of several mm (7-8 mm at maximum) in horizontal direction and grains might have dispersed randomly within a packet, there may be difference in neutron flux between grains even in a single packet. If some grains are exposed to a larger flux of fast neutrons than other grains, a larger amount of ^{39}Ar is produced from the ^{39}K and calculated ages should be younger. Ongoing experiments suggest there is surely a horizontal gradient in neutron flux across the capsule in the reactor. Further study is necessary to solve the problem.

As a conclusion, we obtained reproducible results for the repeated single grain analyses of FC3 biotite, while we identified the heterogeneity in ages among the grains of Sori biotite. Our experimental precision by repeated analyses could be better than 0.5%.

5.3 Total fusion analyses of two age-known biotite samples

Biotites (200–300 μm in diameter) separated from two Neogene volcanic rocks were dated by the single grain total fusion analysis. One sample is biotite separated from the Muro volcanic rock (ISE 9404) whose K–Ar age is 14.44±0.16 Ma (Uto *et al.*, 1997). Thirteen analyses of this biotite give a weighted mean age of 14.31±0.04 Ma (Fig. 11a; Table 5), which is concordant with the K–Ar age. Four ages with the lowest uncertainties tightly cluster around the weighted mean age, and other 9 ages are also concordant with the weighted mean age within 2σ uncertainties. Relative probability distribution spec-

trum for this biotite, thus, forms a single peak and suggests that all individual analyses are acceptable and that none of this biotite is xenocrystic nor thermally disturbed.

Another sample is TRG04 biotite separated from the Utaosa rhyolite of the Teragi Group distributed in Southwest Japan. A K–Ar age of this biotite has been reported to be 2.48±0.02 Ma (Uto *et al.*, 1994). Eight analyses of one to two grains of this biotite yielded a weighted mean age of 2.52±0.02 Ma (Fig. 11b; Table 5), which is in perfect agreement with the K–Ar age. The youngest and the oldest ages have large analytical uncertainties due to small sample sizes. Other six ages are tightly clustered around the weighted mean age. Relative probability distribution spectrum, thus, is a symmetrical single peak.

These results confirmed that the single grain dating of biotite as young as 2.5 Ma can yield highly precise and reliable ages.
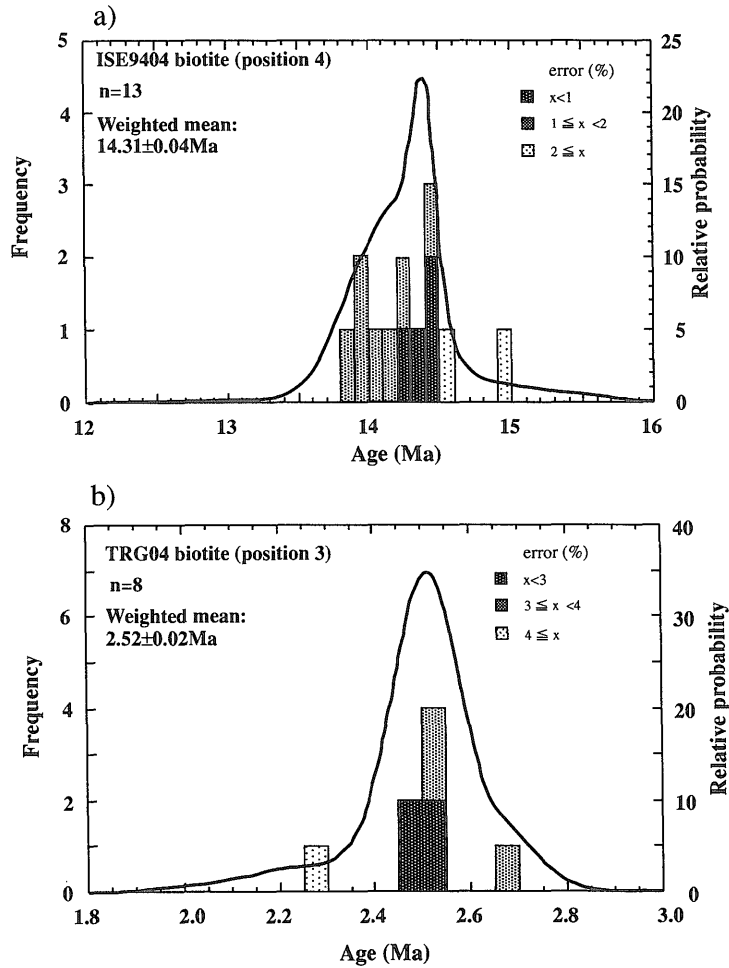

Fig. 11 Single grain analyses of age-known Neogene biotites.
a) Biotite separated from the Muro Volcanic Rock (K–Ar age: 14.44±0.16 Ma). b) Biotite separated from the Utaosa Rhyolite (K–Ar age: 2.48±0.02 Ma). Solid curves depict relative probability distribution spectra.

Table 5 Analytical data for total fusion analysis of Neogene biotite

$^{40}Ar/^{39}Ar$	$^{37}Ar/^{39}Ar$ (x10^{-3})	$^{36}Ar/^{39}Ar$ (x10^{-3})	$^{37}Ar_{Ca}/^{39}Ar_K$ (x10^{-3})	$^{40}Ar^*$ (%)	$^{40}Ar^*/^{39}Ar_K$	Age (Ma)
ISE9404 biotite (Muro volcanic rock); J=0.003732±0.000007 (position No. 4)						
2.324±0.004	2.836±0.419	0.5862±0.0449	2.800	92.5	2.147±0.014	14.40±0.09
2.326±0.002	20.14±0.21	0.6119±0.0357	20.14	92.3	2.144±0.011	14.38±0.07
2.336±0.004	10.50±3.34	0.8572±0.1023	10.50	89.2	2.081±0.031	13.96±0.20
2.443±0.020	38.45±1.34	1.000±0.041	38.45	88.1	2.148±0.012	14.41±0.08
2.327±0.004	<1	0.7046±0.1225	<1	91.0	2.115±0.036	14.19±0.24
2.499±0.004	1.879±20.564	0.9094±0.3335	1.879	89.2	2.227±0.099	14.93±0.66
2.478±0.003	6.125±5.506	1.176±0.090	6.125	86.0	2.128±0.027	14.27±0.18
2.501±0.003	2.422±7.143	1.397±0.133	2.422	83.5	2.085±0.039	13.98±0.26
2.480±0.003	1.653±5.137	1.378±0.098	1.653	83.6	2.070±0.029	13.88±0.19
3.290±0.005	44.72±4.63	3.854±0.109	44.73	65.5	2.152±0.032	14.43±0.22
2.875±0.004	17.35±11.97	2.384±0.261	17.35	75.5	2.169±0.077	14.55±0.52
2.715±0.022	10.04±4.24	2.096±0.070	10.04	77.2	2.094±0.028	14.04±0.19
3.063±0.002	83.12±3.35	3.222±0.056	83.13	69.2	2.117±0.017	14.20±0.11
					Weighted mean	**14.31±0.04**
TRG04 biotite (Utaosa rhyolite); J=0.003736±0.000007 (position No. 3)						
0.5886±0.0007	0.6394±0.2337	0.7098±0.0260	0.6394	54.2	0.3756±0.0079	2.53±0.05
0.9245±0.0009	0.4033±0.2033	1.870±0.026	0.4033	40.0	0.3686±0.0080	2.48±0.05
0.8966±0.0008	0.3320±0.2114	1.750±0.027	0.3320	42.1	0.3764±0.0080	2.54±0.05
0.6276±0.0008	<0.1	0.8430±0.0403	<0.1	60.1	0.3752±0.0120	2.53±0.08
0.5693±0.0012	0.6317±0.2097	0.5736±0.0350	0.6317	70.1	0.3966±0.0105	2.67±0.07
1.013±0.001	0.5557±0.0527	2.186±0.030	0.5557	36.0	0.3640±0.0092	2.45±0.06
0.6534±0.0011	0.2359±0.1693	0.9365±0.0448	0.2360	57.4	0.3734±0.0134	2.51±0.09
1.171±0.002	<0.1	2.822±0.0746	<0.1	28.6	0.3339±0.0221	2.25±0.15
					Weighted mean	**2.52±0.02**

Corrected for decay and blank. All errors listed at the 1σ level.

$(^{40}Ar/^{39}Ar)_K$=0.003258±0.001700; $(^{38}Ar/^{39}Ar)_K$=0.05692±0.00027

$(^{39}Ar/^{37}Ar)_{Ca}$=0.0008370±0.0000069; $(^{36}Ar/^{37}Ar)_{Ca}$=0.0003669±0.0000020

5.4 Stepwise heating analysis of Sori biotite

Several stepwise heating experiments were performed on Sori biotite using two grains each (Table 6), and reproducible age spectra were obtained from all experiments. Typical age spectra of these analyses are shown in Fig. 12. The first 2 to 3 steps at lower laser output (lower temperatures) give younger ages than the K-Ar age. Ages increased with increasing the laser power. Successive 5 to 7 steps at higher temperatures give concordant ages within 2σ error and form a plateau including 70 to 80% of total released ^{39}Ar. The plateau ages of 92.0±0.3 Ma and 92.8±0.3 Ma are about 1 million years older than the K-Ar age. On the other hand, integrat-

ed ages including all released gas fractions, 91.4±0.3 and 91.2±0.2 Ma are in good agreement with the K-Ar age as was the case of total fusion analyses (Table 4). Chloritization along the cleavages of Sori biotite could be responsible for the younger age spectra in the lower temperature steps, while the plateau ages about 1 million years older than the integrated and total fusion ages indicate the primary age of the biotite. Based on these analyses, the age when Sori granodiorite cooled down to the blocking temperature of biotite at about 300°C is considered to be around 92.5 Ma, which is about 1 million years older than that has been thought before. These analyses of Sori biotite clearly indicate

Table 6 Analytical data for stepwise heating analysis of Sori biotite

Laser ouput (W)	$^{40}Ar/^{39}Ar$	$^{37}Ar/^{39}Ar$ (x10⁻³)	$^{36}Ar/^{39}Ar$ (x10⁻³)	$^{40}Ar*$ (%)	$^{39}Ar_K$ fraction (%)	$^{40}Ar*/^{39}Ar_K$	Age (Ma)
Sori biotite (M9512); J=0.003778±0.000008							
0.05	17.68±0.17	<3	29.30±7.32	51.0	0.52	9.002±2.162	60.34±14.25
0.15	14.26±0.02	26.95±2.95	2.656±0.187	94.5	16.72	13.45±0.06	89.44±0.42
0.25	14.07±0.02	<3	0.6445±0.0588	98.6	30.60	13.85±0.04	92.04±0.24
0.40	14.10±0.02	20.44±4.93	0.7077±0.0865	98.8	31.56	13.88±0.04	92.17±0.25
0.60	13.93±0.22	108.6±8.9	0.6861±0.1703	98.6	13.71	13.72±0.22	91.16±1.45
0.90	13.98±0.05	533.5±16.9	<0.4	100.0	3.96	14.03±0.18	93.16±1.13
fusion	13.65±0.04	236.9±32.3	<0.4	100.0	2.92	13.66±0.31	90.79±2.00
Sori biotite (M9513); J=0.003778±0.000008							
0.05	19.32±0.09	<3	42.31±3.26	35.2	0.94	6.793±0.962	45.71±6.39
0.10	13.56±0.05	<3	8.467±1.273	81.5	3.63	11.03±0.38	73.66±2.48
0.15	14.23±0.03	<3	1.751±0.013	96.4	25.71	13.69±0.05	90.97±0.34
0.20	14.07±0.03	8.633±9.326	0.4490±0.1127	99.9	25.54	13.92±0.05	92.46±0.34
0.25	14.24±0.03	<3	0.9192±0.2541	98.1	13.95	13.95±0.08	92.63±0.54
0.30	14.27±0.04	<3	1.408±0.845	97.1	6.34	13.83±0.25	91.87±1.65
0.40	14.34±0.03	57.17±15.12	0.5879±0.3299	98.8	10.94	14.15±0.11	93.94±0.68
0.50	14.13±0.05	40.80±40.81	<0.4	100.0	4.55	14.12±0.14	93.74±0.92
0.80	14.11±0.06	47.74±62.67	0.4163±0.6752	99.2	3.49	13.97±0.21	92.79±1.36
fusion	14.19±0.04	1497±35	1.512±0.707	98.2	4.91	13.94±0.22	92.56±1.39

Corrected for decay and blank. All errors listed at the 1σ level excluding the error of J value.

$(^{40}Ar/^{39}Ar)_K$=0.02308±0.002374;

$(^{39}Ar/^{37}Ar)_{Ca}$=0.000604±0.000022; $(^{36}Ar/^{37}Ar)_{Ca}$=0.000449±0.000096

that the stepwise heating experiment of biotite can yield more geologically meaningful ages with higher precision.

5.5 Stepwise heating analysis of ground-mass of volcanic rocks

In order to know the precise and meaningful ages of altered and/or subaqueous volcanic rocks, the stepwise heating experiment is very promising tool. We must stepwisely extract argon gas of samples in more than 8 to 10 fractions in order to get meaningful plateau or iso-chron ages. It is, thus, important to homogeneously heat a large size of sample espe-cially in the case of young volcanic rocks which have accumulated only a small amount of radiogenic ^{40}Ar. It is very difficult for most laboratories to homogeneously heat the sample larger than a few micrometers in diameter as has mentioned in chapter 3.5, but the laser $^{40}Ar/^{39}Ar$ system at the Geological Survey of Japan is capable of creating a energetically flat beam to homogeneously heat a sample up to a few milli-meter in diameter.

We preliminary dated a groundmass fragment of about 2 milligram of a Miocene basalt lava. The sample, MAT8714, was taken from the Takashibiyama Formation, distributed in the northern Shimane Peninsula, Southwest Japan. Its conventional K-Ar age is 9.7±1.6 Ma (Uto, 1989). From the viewpoint of the field stratigra-phy, this formation could be contemporaneous with the Matsue Formation distributed dis-continuously about 10 km south (Kano and Yoshida, 1985). Several available K-Ar ages for the Matsue Formation are all clustered around 11-12 Ma, which are not inconsistent with the age of MAT8714 within the experimen-tal errors, but the current age information is not strong enough to support the interpretation of Kano and Yoshida (1985). Age spectrum for MAT8714 is shown in Fig. 13. Twelve steps out of 13 steps give concordant ages within 2σ error and yield a plateau age of 12.09±0.19 Ma. The $^{37}Ar_{Ca}/^{39}Ar_K$ ratio increases with increasing the temperature of extraction, indicating that K-rich phases like K-rich feldspars and glass
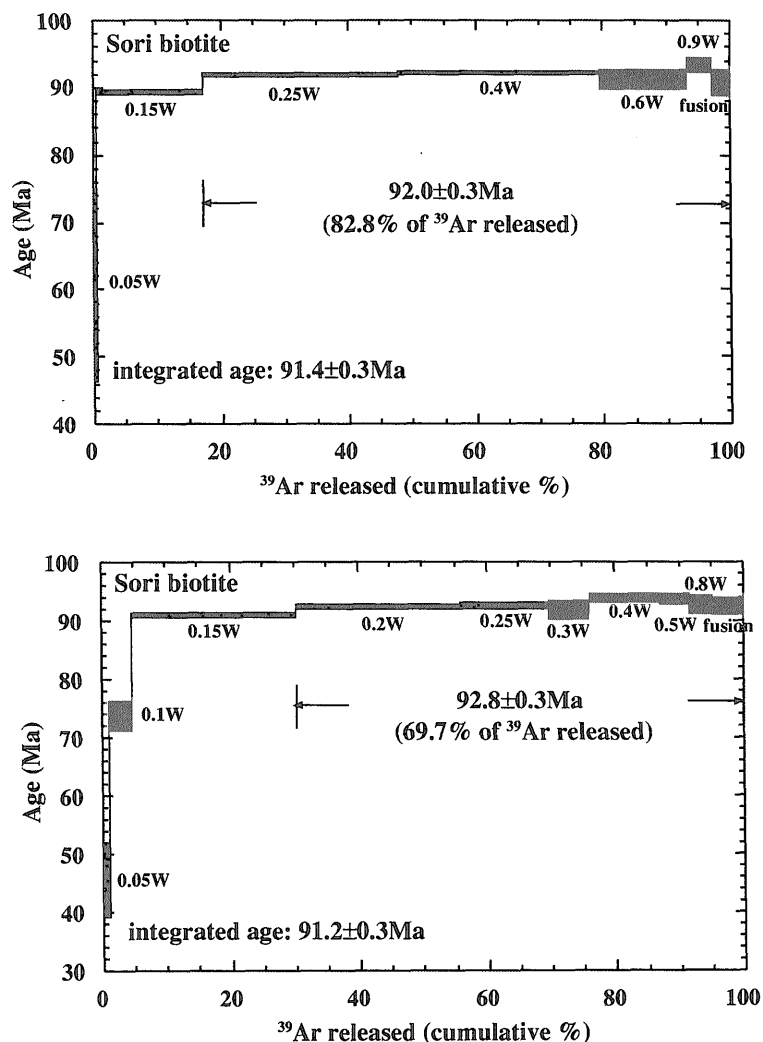
Fig. 12 Age spectra for Sori biotite.

Two grains of Sori biotite were analyzed in each experiment. Height of each box indicates the error for analysis of each step (1σ). Laser output for each step is also shown in wattage.

Table 7 Analytical data for stepwise heating analysis of groundmass of Miocene volcanic rocks (MAT8714) (position No. 13)

Laser ouput (W)	$^{40}Ar/^{39}Ar$	$^{37}Ar/^{39}Ar$ (x10³)	$^{36}Ar/^{39}Ar$ (x10³)	$^{37}Ar_{Ca}/^{39}Ar_{K}$ (x10³)	$^{40}Ar^{*}$ (%)	$^{39}Ar_{K}$ fraction (%)	$^{40}Ar^{*}/^{39}Ar_{K}$	Age (Ma)
0.20	139.6±0.5	418.9±6.4	472.8±2.1	419.1	n.d.	2.11	<0.5	<3.4
0.25	24.89±0.05	1982±9	79.09±0.67	1985	6.9	4.71	1.732±0.197	11.63±1.32
0.40	28.92±0.04	676.4±5.8	92.08±0.52	676.8	6.1	7.01	1.777±0.149	11.93±1.00
0.50	24.05±0.03	965.0±3.7	76.20±0.39	9658	6.8	7.58	1.640±0.113	11.02±0.76
0.65	16.46±0.04	1580±5	50.49±0.37	1583	10.4	6.65	1.713±0.105	11.51±0.70
0.80	18.30±0.04	2213±10	55.88±0.59	2218	10.1	6.13	2.032±0.172	13.64±1.15
1.00	18.04±0.02	2639±5	56.07±0.29	2645	9.7	12.42	1.752±0.084	11.77±0.56
1.25	13.00±0.03	2783±7	38.97±0.26	2790	13.7	13.26	1.789±0.077	12.01±0.52
1.50	10.18±0.01	2689±5	29.02±0.26	2695	18.6	7.48	1.901±0.078	12.76±0.52
1.80	9.696±0.015	2243±8	27.74±0.28	2248	17.9	5.17	1.743±0.081	11.71±0.54
2.20	8.492±0.011	1873±5	23.47±0.40	1876	20.7	4.46	1.759±0.119	11.81±0.80
2.50	8.628±0.016	1996±5	23.99±0.32	1999	20.3	4.13	1.757±0.093	11.80±0.62
fusion	14.77±0.02	5225±8	45.53±0.11	5248	12.7	18.90	1.885±0.029	12.66±0.19

J=0.003735±0.000007   n.d. = not detectable

Corrected for decay and blank. All errors listed at the 1σ level excluding the error of J value.

$(^{40}Ar/^{39}Ar)_{K}$=0.003258±0.001700; $(^{38}Ar/^{39}Ar)_{K}$=0.05692±0.00027

$(^{39}Ar/^{37}Ar)_{Ca}$=0.0008370±0.0000069; $(^{36}Ar/^{37}Ar)_{Ca}$=0.0003669±0.0000020
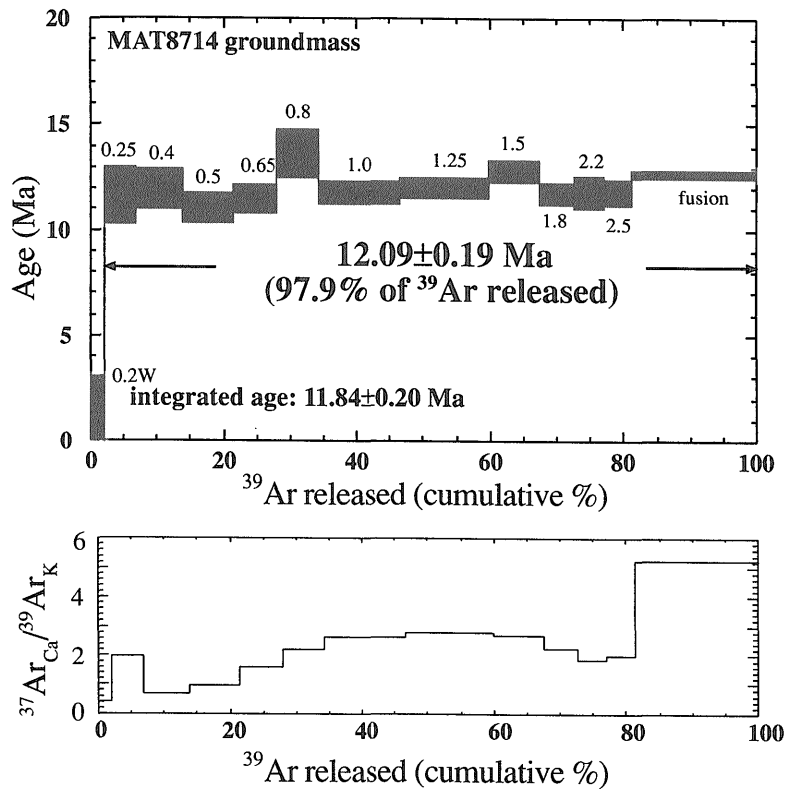
Fig. 13 Age spectrum for a Miocene lava.
About 2 mg groundmass sample of a basalt lava from the Takashibiyama Formation, Southwest Japan, was analyzed. The release profile of $^{37}Ar_{Ca}/^{39}Ar_K$ ratio is also shown in the bottom.

mainly degassed during the lower temperature steps but that Ca-rich phases gradually became dominant in the higher temperature steps. This age is consistent with the K-Ar age considering 2s error, and is identical to the ages of the Matsue Formation. Our preliminary result, thus, support the stratigraphic correlation suggested by Kano and Yoshida (1985). The laser stepwise heating $^{40}Ar/^{39}Ar$ dating is thus confirmed to be a very powerful technique to precisely and accurately date Neogene volcanic rocks.

Conclusions

A laser-heating $^{40}Ar/^{39}Ar$ dating system has been established at the Geological Survey of Japan in order to date very small amounts of minerals and volcanic rocks accurately and precisely. Introduction of optical glass-fiber in the laser optics makes it possible to create a wide but energetically homogeneous laser beam up to 4 millimeters in diameter. Samples larger than a millimeter across can thus be homogeneously heated by this technique, and reliable stepwise heating experiments by the laser heating method particularly for young volcanic rocks have become possible.

Preliminary experiments on biotite standards suggest that not only total fusion dating but also stepweise heating experiments of a single to a few grains give reliable age data. Relative age relationship between Sori and FC3 biotites is perfectly accordant with that of existing K-Ar ages.

Consistent ages were also obtained for two age-known biotite samples from Neogene volcanic rocks by total fusion analyses of one or two phenocryst grains. A weighted mean age for 13 analyses on Muro volcanic rocks (K-Ar age: 14.44±0.16 Ma) is 14.31±0.04 Ma, and that for 7 analyses on Utaosa Rhyolite (2.48±0.02 Ma) is 2.52±0.02 Ma.

A stepwise heating experiment on a millimeter size groundmass grain of a Miocene volcanic rock (K-Ar age: 9.7±1.6 Ma) was also successful and a very reliable plateau age of 12.09±0.19 Ma was obtained as the weighted mean of 12 consecutive steps.

It is thus confirmed that precise and accurate ages of mineral and rock samples less than a few milligrams can be obtained by the established laser heating $^{40}Ar/^{39}Ar$ system at the Geological Survey of Japan.

Reference

Dalrymple, G. B. (1989) The GLM continuous laser system for $^{40}Ar/^{39}Ar$ dating: Description and performance characteristics. *USGS Bull. 1890*, 89-96.

Kano, K., and Yoshida, F. (1985) *Geology of the Sakaiminato district*. Quadrangle Series, scale 1:50,000, Geol.Surv.Japan, 57p. (in Japanese with English abstract 5p.).

Lanphere, M.A., Dalrymple, G.B., Fleck, R.J. and Pringle, M.S. (1990) Intercalibration of mineral standards for K-Ar and $^{40}Ar/^{39}$ Ar measurements. EOS, 71, 1658.

Matsumoto, A. (1989) Improvement for determination of potassium in K-Ar dating. *Bull. Geol.Surv.Japan*, 40, 65-70 (in Japanese with English abstract).

Naser, C.W. and Cebula, G.T. (1985) Re-collection of Fish Canyon Tuff for fission-track standardization. *Nucl.Tracks*, 10, 393.

Pringle, M. S., McWilliams, M., Houghton, B. F., Lanphere, M. A. and Wilson C. J. N. (1992): $^{40}Ar/^{39}Ar$ dating of Quaternary feldspar: Examples from the Taupo Volcanic Zone, New Zealand. Geology, 20, 531-534.

Potts, P.J. (1987) *A handbook of silicate rock analysis*. Blackie & Sons Limited, London, 622p.

Stewart, K., Turner, S., Regelous M., Kelley, S., Hawkesworth, C., Kirstein, L. and Mantovani, M. (1996) 3D $^{40}Ar-^{39}Ar$ geochronology in the Parana continental flood basalt province. *Earth Planet. Sci. Lett.*, 143, 95-109.

Uchiumi, S. and Shibata, K. (1980) Errors in K-Ar age determination. *Bull.Geol.Surv.Japan*, 31, 267-273 (in Japanese with English abstract).

Uto, K. (1989) Neogene volcanism of Southwest Japan: Its time and space based on K-Ar dating. PhD thesis, 184pp., Univ. Tokyo.

Uto, K., Tagami,T. and Uchiumi, S. (1994) K-Ar and fission-track dating on volcanic rocks of Pliocene Teragi Group from eastern San' in region, Southwest Japan. J.Geol.Soc. Japan, 100, 787-798 (in Japanese with English abstract).

Uto, K., Anno, K., Sudo, M., Uchiumi, S. (1997) K-Ar ages for Middle Miocene Muro volcanic rocks, Southwest Japan. Bull.Volcanol.Soc.Japan (in press).

Appendix 1
Correction for blanK

$(^{40}Ar)s = (^{40}Ar)s$

$(^{39}Ar)s = (^{40}Ar)s \cdot (^{39}Ar/^{40}Ar)s$

$(^{38}Ar)s = (^{40}Ar)s \cdot (^{38}Ar/^{40}Ar)s$

$(^{37}Ar)s = (^{40}Ar)s \cdot (^{37}Ar/^{40}Ar)s$

$(^{36}Ar)s = (^{40}Ar)s \cdot (^{36}Ar/^{40}Ar)s$

$(^{40}Ar)b.cor. = (^{40}Ar)s - (^{40}Ar)b$

$(^{39}Ar)b.cor. = (^{39}Ar)s - (^{39}Ar)b$

$(^{38}Ar)b.cor. = (^{38}Ar)s - (^{38}Ar)b$

$(^{37}Ar)b.cor. = (^{37}Ar)s - (^{37}Ar)b$

$(^{36}Ar)b.cor. = (^{36}Ar)s - (^{36}Ar)b$

m : mass number

$(^{m}Ar)s$: : intensity of ^{m}Ar determined in sample analysis

$(^{m}Ar/^{m'}Ar)s$: $^{m'}Ar/^{m}Ar$ ratio determined in sample analysis

$(^{m}Ar)b.$: intensity of ^{m}Ar determined in blank analysis

$(^{m}Ar)b.cor.$: intensity of ^{m}Ar after blank correction

Correction for mass discrimination

$\Delta = (295.5 - (^{40}Ar/^{36}Ar)a) / (^{40}Ar/^{36}Ar)a/4$

$(^{40}Ar)m.cor. = (^{40}Ar)b.cor.$

$(^{39}Ar)m.cor. = (^{39}Ar)b.cor. \cdot (1+\Delta)^{-1}$

$(^{38}Ar)m.cor. = (^{38}Ar)b.cor. \cdot (1+2\Delta)^{-1}$

$(^{37}Ar)m.cor. = (^{37}Ar)b.cor. \cdot (1+3\Delta)^{-1}$

$(^{36}Ar)m.cor. = (^{36}Ar)b.cor. \cdot (1+4\Delta)^{-1}$

Δ : mass discrimination correction factor

$(^mAr/^{m'}Ar)a$: $^mAr/^{m'}Ar$ ratio determined in air analysis

$(^mAr)m.cor.$: intensity of ^mAr after mass discrimination correction

Correction for decay

$(^{39}Ar)d.cor. = (^{39}Ar)m.cor. \cdot 0.5^\wedge(-t/(269 \cdot 365))$

$(^{37}Ar)d.cor. = (^{37}Ar)m.cor. \cdot (1-0.5^\wedge(t'/35.1))) \cdot$
$0.693/35.1 \cdot 0.5^\wedge(t/35.1)$

$(^mAr)d.cor.$: intensity of ^mAr after decay correction

t : time from the end of irradiation to the start of analysis

t' : duration of irradiation

Correction for interfering isotopes

$(^{36}Ar)i.cor. = (^{36}Ar)m.cor. - (^{37}Ar)d.cor. \cdot$
$(^{36}Ar/^{37}Ar)_{ca}$

$(^{39}Ar)i.cor. = (^{39}Ar)d.cor. - (^{37}Ar)d.cor. \cdot$
$(^{39}Ar/^{37}Ar)_{ca}$

$(^{40}Ar)i.cor. = (^{40}Ar)m.cor. - (^{39}Ar)i.cor. \cdot$
$(^{40}Ar/^{39}Ar)_K$

$(^mAr)i.cor.$: intensity of ^mAr after correction for interfering isotopes

$(^mAr/^{m'}Ar)_{ca}$: $^mAr/^{m'}Ar$ ratio determined in analysis of CaF_2:

$(^mAr/^{m'}Ar)_K$: $^mAr/^{m'}Ar$ ratio determined in analysis of $KFeSiO_4$

Calculation of $^{40}Ar^*$ and $^{39}Ar_K$

$^{40}Ar^* = (^{40}Ar)i.cor. - (^{40}Ar)a$
$= (^{40}Ar)i.cor. - 295.5 \cdot (^{36}Ar)i.cor.$

$^{39}Ar_K = (^{39}Ar)i.cor.$

$^{40}Ar^*$: intensity of radiogenic ^{40}Ar

$^{39}Ar_K$: intensity of potassium-derived ^{39}Ar

$(^{40}Ar)a$: intensity of atmospheic ^{40}Ar

Calculation of age

$T = 1/\lambda \cdot \ln (1 + (^{40}Ar^*/^{39}Ar_K) \cdot J)$

T : age

λ : decay constant for ^{40}K

J : J value

Calculation of J value

$J = ((\exp \lambda T_f) - 1)/(^{40}Ar^*/^{39}ArK)f$

Tf : age of flux monitor mineral

$(^{40}Ar^*/^{39}Ar_K)f$: $^{40}Ar^*/^{39}Ar_K$ ratio dertermined in analysis of flux monitor mineral

Appendix 2

Error for correction of blanK

$\sigma(^{40}Ar)b.cor. = ((\sigma(^{40}Ar)s)^\wedge2 + (\sigma(^{40}Ar)b)^\wedge2)^\wedge$
0.5

$\sigma(^{39}Ar)b.cor. = ((\sigma(^{39}Ar)s)^\wedge2 + (\sigma(^{39}Ar)b)^\wedge2)^\wedge$
0.5

$\sigma(^{38}Ar)b.cor. = ((\sigma(^{38}Ar)s)^\wedge2 + (\sigma(^{38}Ar)b)^\wedge2)^\wedge$
0.5

$\sigma(^{37}Ar)b.cor. = ((\sigma(^{37}Ar)s)^\wedge2 + (\sigma(^{37}Ar)b)^\wedge2)^\wedge$
0.5

$\sigma(^{36}Ar)b.cor. = ((\sigma(^{36}Ar)s)^\wedge2 + (\sigma(^{36}Ar)b)^\wedge2)^\wedge$
0.5

$\sigma(^mAr)s$: error for intensity of ^mAr determined in sample analysis

$\sigma(^mAr)b$: error for intensity of ^mAr determined in blank analysis

$\sigma(^mAr)b.cor.$: error for intensity of ^mAr determined in blank analysis

Error for correction of interfering isotopes

$\sigma(^{40}Ar)i.cor. = ((\sigma(^{40}Ar)m.cor.)^\wedge2 + (((\sigma$
$(^{39}Ar)d.cor./(^{39}Ar)d.cor.)^\wedge2 +$
$(\sigma(^{40}Ar/^{39}Ar)K/(^{40}Ar/^{39}Ar)K)^\wedge$
$2)^\wedge0.5)((^{39}Ar)d.cor.)(^{40}Ar/$
$^{39}Ar)K)^\wedge2)^\wedge0.5$

$\sigma(^{39}Ar)i.cor. = ((\sigma(^{39}Ar)d.cor.)^\wedge2 + (((\sigma(^{37}Ar)$
$d.cor./(^{37}Ar)d.cor.)^\wedge2 + (\sigma$
$(^{39}Ar/^{37}Ar)_{ca}/(^{39}Ar/^{37}Ar)_{ca})^\wedge2)^\wedge$
$0.5)((^{37}Ar)d.cor.) \cdot (^{39}Ar/$
$^{37}Ar)_{ca})^\wedge2)^\wedge0.5$

$\sigma(^{38}Ar)i.cor. = ((\sigma(^{38}Ar)m.cor.)^\wedge2 + (((\sigma$
$(^{39}Ar)d.cor./(^{39}Ar)d.cor.)^\wedge2 +$
$(\sigma(^{38}Ar/^{39}Ar)_K/(^{38}Ar/^{39}Ar)_{ca})^\wedge$
$2)^\wedge0.5) \cdot ((^{39}Ar)d.cor.) \cdot (^{38}Ar/$
$^{39}Ar)_K)^\wedge2)^\wedge0.5$

$\sigma(^{36}Ar)i.cor. = ((\sigma(^{36}Ar)m.cor.)^\wedge2 + (((\sigma$
$(^{36}Ar)d.cor./(^{37}Ar)d.cor.)^\wedge2 +$
$(\sigma(^{36}Ar/^{37}Ar)_{ca}/(^{36}Ar/^{37}Ar)_{ca})^\wedge$
$2)^\wedge0.5) \cdot ((^{37}Ar)d.cor.) \cdot (^{36}Ar/$
$^{37}Ar)_{ca})^\wedge2)^\wedge0.5$

$\sigma(^mAr)i.cor.$: error for intensity of ^mAr after correction for interfering isotopes

$\sigma(^mAr)m.cor.$: error for intensity of ^mAr after mass discrimination correction

$\sigma(^mAr)d.cor.$: error for intensity of ^mAr after

mass decay correction

$\sigma(^mAr/^{m'}Ar)_{Ca}$: error for $^mAr/^{m'}Ar$ ratio determined in analysis of CaF_2

$\sigma(^mAr/^{m'}Ar)_K$: error for $^mAr/^{m'}Ar$ ratio determined in analysis of $KFeSiO_4$

Error for $^{40}Ar^*$ and $^{39}Ar_K$

$$\sigma(^{40}Ar^*) = (\sigma(^{40}Ar)i.cor.)\hat{\ }2 + (295.5 \cdot \sigma(^{36}Ar)i.cor.)\hat{\ }2$$

$$\sigma(^{39}Ar_K) = \sigma(^{39}Ar)i.cor.$$

$\sigma(^{40}Ar^*)$: error for intensity of radiogenic ^{40}Ar

$\sigma(^{39}Ar_K)$: error for intensity of potassium-derived ^{39}Ar

Error for age

$$\sigma(T) = (((\sigma(^{40}Ar^*)/^{40}Ar^*)\hat{\ }2 + (\sigma(^{39}Ar_K)/^{39}Ar_K)\hat{\ }2 + \sigma(J)\hat{\ }2)\hat{\ }0.5) \cdot T$$

$\sigma(T)$: error for age

$\sigma(J)$: error for J value

地質調査所のレーザ加熱$^{40}Ar／^{39}Ar$年代測定システム：

システムの概要と予察的測定結果

宇都浩三・石塚　治・松本哲一・上岡　晃・富樫茂子

要　旨

　地質調査所において$^{40}Ar/^{39}Ar$年代測定システムを確立した．このシステムの主眼は，レーザ加熱法により，鉱物一粒子や数mg以下の火山岩の年代測定を行うことである．システムはアルゴン同位体実験室，レーザ抽出系，希ガス専用質量分析計及び操作卓の４つの部分により構成される．地質調査所におけるレーザ抽出系の大きな特徴は，レーザビームを試料チャンバーに導入する光学系に，光ファイバー及び光学顕微鏡を採用していることである．この方式により，試料表面に均質なエネルギー分布を持つ最大4mmまでのレーザビームを得ることができる．そのため，径が2-3mmの試料でも均質に加熱することが可能である．黒雲母標準試料についての予察的測定結果は，全融解年代測定だけでなく，１ないし数粒子の段階加熱測定でも，十分信頼性の高い年代が得られることが示された．標準試料である沢入黒雲母とFC3黒雲母について得られた年代値の相対的関係は，K-Ar法により求められているものと完全に一致した．また新第三紀火山岩から分離された黒雲母1-2粒子を用いた全融解法による測定により，既存のK-Ar年代と調和的な年代が得られた．室生火山岩類（K-Ar年代：14.44±0.16Ma）についての13測定の加重平均値として14.31±0.04Ma，また歌長流紋岩（K-Ar年代：2.48±0.02Ma）についての7測定の加重平均値として2.52±0.02Maを得た．さらに，中新世の火山岩（K-Ar年代：9.7±1.6Ma）の段階加熱測定においても，連続した12ステップの加重平均値として12.09±0.19Maのプラトー年代が得られた．

Plate. 1   Outline of ^{40}Ar/^{39}Ar dating system.
    All the equipments are placed in a radioisotope laboratory that is regulated by the law. Laser head and laser optics are placed in the safety box. Purification line (right of the safety box) is connected with the noble gas mass spectrometer (front right). Operation desk (front left) is for the remote control of the system.

Plate 2   Laser optics
    Laser beam emitted from a 10W continuous Ar-ion laser passes through the optical glass fiber (black cable connected with the microscope) and then introduced into the optical microscope. Then, the beam comes out through the objective lens and penetrates into the ultra high-vacuum sample chamber (below the objective lens in the center of the figure) to heat the sample inside.
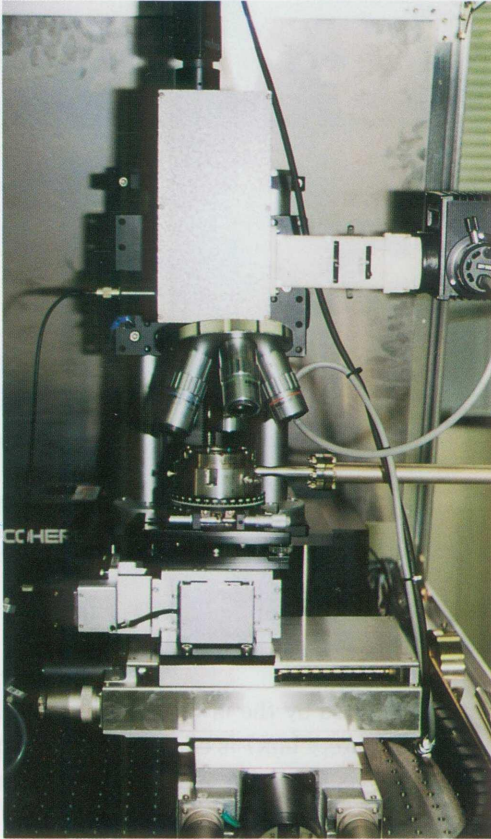
Plate 3   Sample chamber.

   The blue Ar-ion laser beam is emitted to the sample. Single to several grains of samples are loaded in holes drilled on the surface of the copper-made sample holder sit inside the chamber.
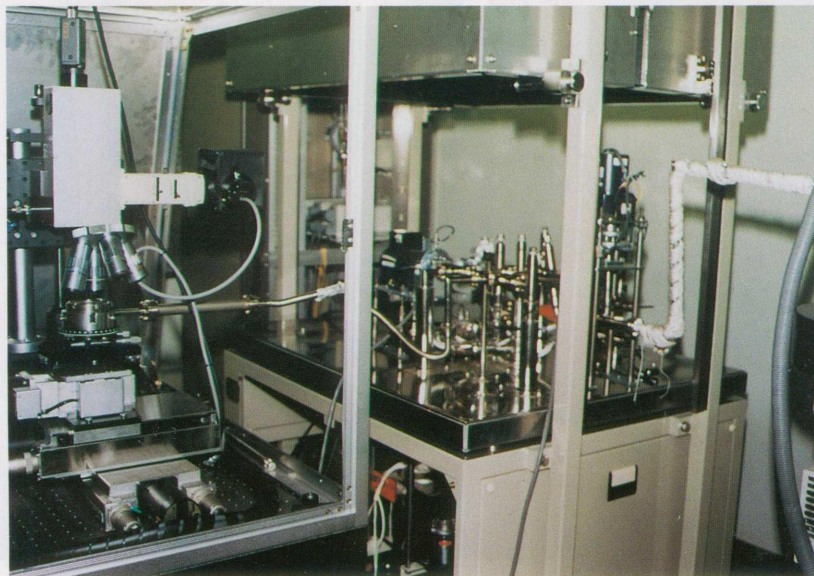

Plate 4   Purification line.

   Gases extracted from the sample chamber (left) are diffused into the purification line (center) through the stainless pipe. The line is equipped with two Zr-Al getters for the purification of active gases. There are two torque motors attached to the valves for the remote operation. One is for the isolation of the ion pump and the other is for the introduction of argon gas to the mass spectrometer. A box above the purification line is an oven for the bakeout of the entire purification line. The line is connected with the mass spectrometer through a stainless pipe (pipe covered with white flexible heater seen in the right end).
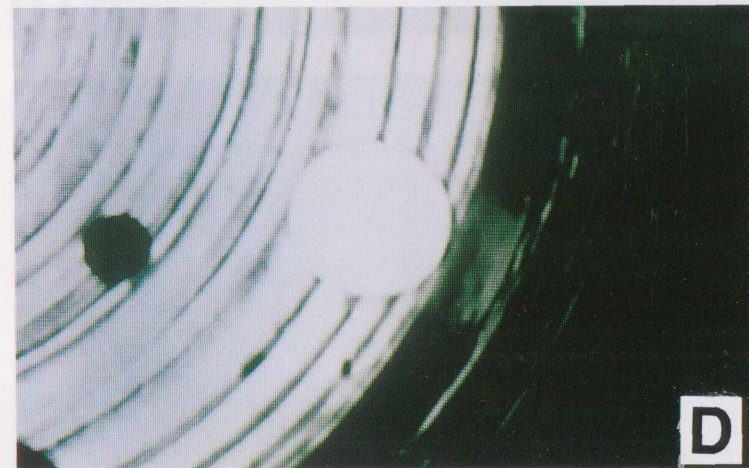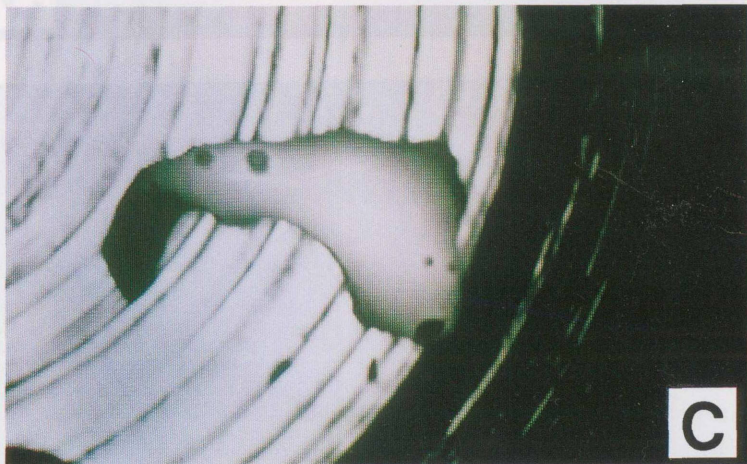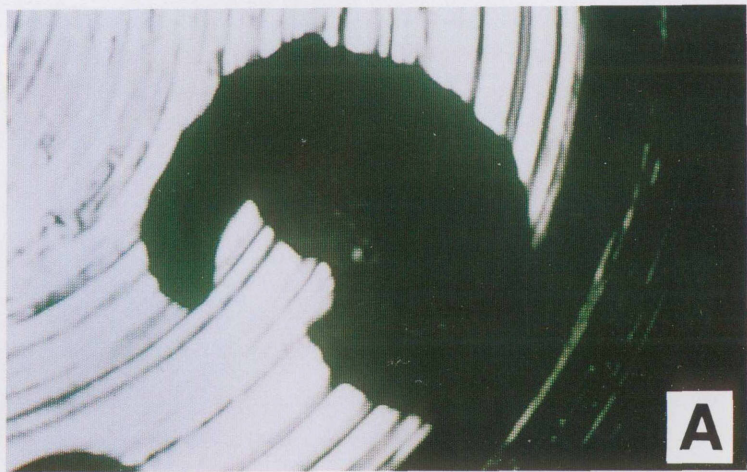
Plate 5   Image of a biotite crystal observed on the display during the total fusion analysis. With increasing the power of the laser (A to D), temperature of the sample gradually increased and the sample started to vesiculate (C). The sample completely melted forming a spherule (D).
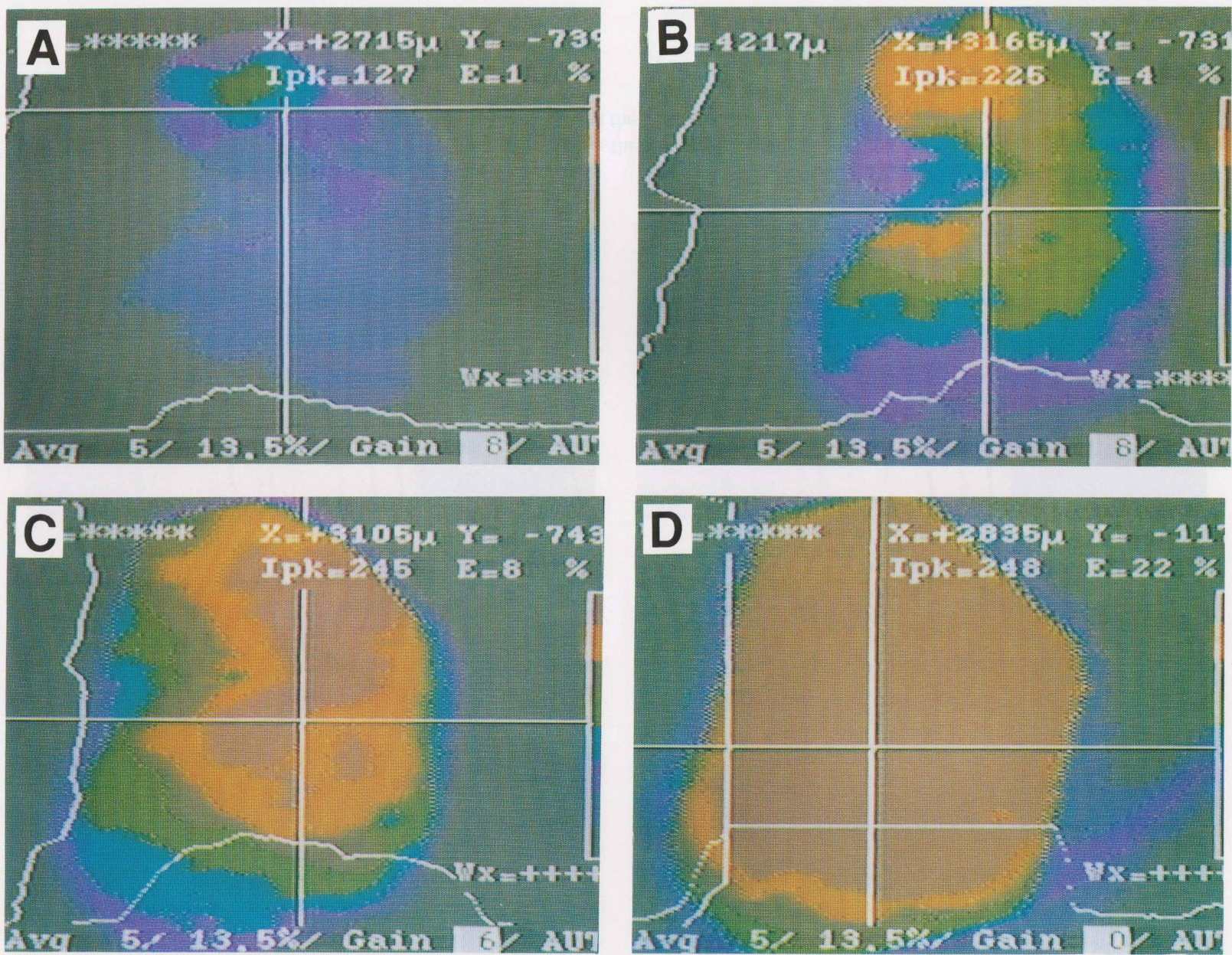
Plate 6   Distribution of the thermal energy of a single biotite crystal during the laser-fusion analysis monitored by the beam profiler.
Warmer colors indicate the area having the higher intensity of IR radiation and the higher thermal energy.